Proceedings of the Sixteenth (2006) International Offshore and Polar Engineering Conference
San Francisco, California, USA, May 28-June 2, 2006

ISBN 1-880653-66-4 (Set); ISSN 1098-6189 (Set)

Numerical Modeling of Extreme Wave Slamming on Cylindrical Offshore Support Structures

Carsten Corte[1], *Stéphan T. Grilli*[2]
[1]Institut für Stahlbau, Technische Universität Braunschweig.
Braunschweig, Germany
[2]Department of Ocean Engineering, University of Rhode Island (URI).
Narragansett, RI, USA

ABSTRACT

In this paper, we study the impact on cylindrical piles of extreme waves (freak waves), generated by directional wave focusing. Waves are numerically modeled based on a boundary element discretization of fully nonlinear potential flow equations with free surface evolution. Higher-order boundary elements are used for the spatial discretization, and a higher-order time integration scheme based on the Taylor series expansion is applied.
We model the pressure impact of a freak wave on a cylindrical offshore support structure, as the slamming process of a wave front around a circular cross-section, by a finite volume – volume of fluid approach. Results are analyzed in detail and compared to an analytic solution and to experimental results. Finally, the full loading on a cylindrical tower structure, due to a freak wave, is determined.

KEY WORDS: Freak waves, fully nonlinear potential flow, boundary element method, wave slamming, pressure impact, finite volume - volume of fluid method, tower support structures

INTRODUCTION

An important phenomenon for the design of offshore structures is the appearance of extreme waves at sea, also known as freak waves, which can cause severe damage to offshore structures and ships. In recent years, numerical models have been developed to simulate ocean waves based on the fully nonlinear free surface potential flow equations (FNPF). Initially, such models have been developed to simulate two-dimensional (2D) wave evolution. For instance, Grilli and Subramanya (1994, 1996) developed a 2D-model based on a higher-order boundary element method (BEM), with a second-order mixed Eulerian-Langrangeian time integration scheme. More recently, three-dimensional (3D) numerical wave tanks (NWT) have been developed. Among those, Grilli et al. (2001) proposed a similar algorithm for the 3D solution of FNPF equations, based on a higher-order BEM model.

Freak waves can occur in all regimes of water depth. These are waves highly localized in space and time. Although their probability of appearance is low, they can be extremely dangerous for structures located in their path. Although they are not fully explained yet, it has been shown that freak waves can result from local energy focusing enhanced by nonlinear effects. One of the most commonly proposed mechanisms to explain the appearance of freak waves is directional focusing. Grilli and Brandini (2001) simulated directional wave focusing in a 3D-NWT by specifying an analytically expressed snake wavemaker motion at the inflow boundary, as well as using an absorbing wavemaker motion at the outflow boundary. Alternatively, freak waves can occur due to specific bottom topography or wave-current interactions. Other causes for the appearance of freak waves are wave-wave interaction or particular atmospheric conditions. A summary of freak wave generation mechanisms is given by Kharif and Pelinovsky (2003).
Characteristics of freak waves caused by directional focusing have recently been analyzed by Grilli et al. (2005) and Fochesato et al. (2005ab) using an improved higher-order BEM-model, both more accurate and more efficient. Thus, to reduce the computational cost these authors implemented a Fast Multipole Algorithm (FMA) in the BEM spatial solver. Computational results for the formation of an extreme wave show (i) in a first stage the appearance of a crescent shaped wave crest during the evolution of the wave focusing and (ii) in a second stage, at focusing, an enhanced height in the middle, preceding the formation of the resulting breaker jet.

When wave slamming occurs on a cylindrical support structure, the structure is subjected to short-duration very high impact pressures and forces. Several analytic approaches have been proposed to estimate such transient pressure distribution around the circumference of a circular cross-section and thus the resulting force on the considered structure. These methods are based on the incompressible one-phase potential flow equations, and were first applied by Wagner (1932) to model impact forces during the landing stage of water planes. Fabula (1957) and Goda (1960) show applications for the case of a circular cross-section being impacted by a two-dimensional water front. One of the newest models in this line of work is that of Wienke (2001). All of these methods exhibit a pressure singularity at the beginning of the slamming process, likely due to the assumption of incompressible one-phase flow. Furthermore, these models have been developed for the impact of an even height water front only, which is not valid any more in the case of 3D extreme waves, which arise from directional focusing.

In this paper, to avoid the spurious initial pressure singularity, we use a two-phase flow (water-air) model, which yields a continuous increase in pressure since in the applied model there is no density unsteadiness in space and time. The two-phase flow is assumed to be viscous and governed by the Navier-Stokes equations. The discretization of the Navier-Stokes equations is achieved by a finite volume approach (FV). The representation of the free surface is described by a scalar field variable – the volume fraction – and the temporal evolution of this scalar quantity is described by an advection equation (volume of fluid method, VOF). To validate this finite volume – volume of fluid approach (FV-VOF), for the purpose of modeling the slamming process of waves on support structures, we first solve the case of an even height water front slamming onto a circular cross-section (2D case). Computational results of the FV-VOF method are compared to an analytic solution and to experimental results.

Finally, the transient load on a cylindrical tower structure is determined by using the 3D-BEM model to derive an extreme wave event and initialize computations in the 3D-FV-VOF model, which is then used to compute the transient load on the tower structure.

WAVE MECHANICS

The wave induced flow is described by potential flow equations, whose governing equation is Laplace's equation in domain $\Omega(t)$:

$$\Delta\Phi = 0 \quad in\ \Omega(t) \tag{1}$$

where Φ is the velocity potential and the velocity vector is defined as $\mathbf{u}=\nabla\Phi$. A typical 3D model domain $\Omega(t)$ for the NWT is shown in figure 1.

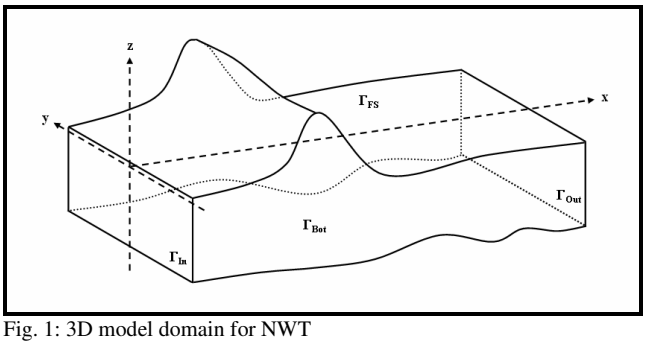

Fig. 1: 3D model domain for NWT

The governing potential equation can be transformed to its boundary representation, which takes the following form:

$$\alpha(\mathbf{x}_c)\Phi(\mathbf{x}_c) = \int_\Gamma \left[\frac{\partial\Phi(\mathbf{x})}{\partial n} G(\mathbf{x},\mathbf{x}_c) - \Phi(\mathbf{x}) \frac{\partial G(\mathbf{x},\mathbf{x}_c)}{\partial n} \right] d\Gamma \tag{2}$$

where $\mathbf{x}_c$ is a collocation point, α_c the boundary factor at location $\mathbf{x}_c$, $G(\mathbf{x}, \mathbf{x}_c)$ is the appropriate Green's function and $\partial / \partial n$ denotes the outwards normal derivative on Γ. On the free surface the kinematic (KFSBC) and dynamic (DFSBC) free surface boundary conditions have to be satisfied as:

$$\frac{D\mathbf{r}}{Dt} = \nabla\Phi \quad on\ \Gamma_{FS}(t) \tag{3}$$

$$\frac{D\Phi}{Dt} = -gz + \frac{1}{2}\nabla\Phi\cdot\nabla\Phi - \frac{p_a}{\rho} \quad on\ \Gamma_{FS}(t) \tag{4}$$

where $\frac{D}{Dt} = \frac{\partial}{\partial t} + \mathbf{u}\cdot\nabla$ is the total derivate with respect to time and $\mathbf{r}$ is a point on $\Gamma_{FS}(t)$. On the outflow, bottom, and inflow boundaries, $\Gamma_{Out}(t)$, $\Gamma_{Bot}(t)$ and $\Gamma_{In}(t)$, respectively, the following Neumann boundary conditions have to hold:

$$\bar{q}(\mathbf{x},t) = \overline{\frac{\partial\Phi}{\partial n}} = q_{Out}(\mathbf{x},t) \quad on\ \Gamma_{Out}(t) \tag{5}$$

$$\bar{q}(\mathbf{x},t) = \overline{\frac{\partial\Phi}{\partial n}} = 0 \quad on\ \Gamma_{Bot}(t) \tag{6}$$

$$\bar{q}(\mathbf{x},t) = \overline{\frac{\partial\Phi}{\partial n}} = q_{In}(\mathbf{x},t) \quad on\ \Gamma_{In}(t) \tag{7}$$

where $q_{In}(\mathbf{x},t)$ and $q_{Out}(\mathbf{x},t)$ are specified time-dependent velocity distributions, and $q(\mathbf{x},t)$ denotes Neumann boundary condition values.

DISCRETIZATION

Spatial discretization

For the discretization of the problem, discrete nodes and two-dimensional surface elements are introduced on the boundary Γ. On each node, discrete values for the velocity potential Φ and the normal outward velocity $q = \partial\Phi / \partial n$ are defined or calculated. Interpolation between nodes is performed by higher-order elements (Grilli and Brandini, 2001). Applying equation (2) for each discrete node on the discretized boundary gives the spatially discretized form of the potential equation. For the element-wise surface integration 16-node bi-cubic elements are defined on the boundary. The surface integration for each part of the boundary is performed for the inner 4-node part of a 16-node element. Then the 16-node element is shifted for the integration of the adjacent part of the boundary. This way of integration is labeled as middle-interval interpolation (MII) element integration.

Time Integration

The time evolution of the free surface in time direction is governed by equations (3, 4). Here, equations are used to derive Taylor series expansion for the free surface position and potential, as follows:

$$\mathbf{r}(t+\Delta t) = \mathbf{r}(t) + \sum_{i=1}^{2} \frac{1}{i!}\Delta t^i \frac{D^i\mathbf{r}(t)}{Dt^i} \quad on\ \Gamma_{FS}(t) \tag{8}$$

$$\Phi(\mathbf{r}(t+\Delta t), t+\Delta t) = \Phi(\mathbf{r}(t),t) + \sum_{i=1}^{2} \frac{1}{i!}\Delta t^i \frac{D^i\Phi(\mathbf{r}(t),t)}{Dt^i} \quad on\ \Gamma_{FS}(t) \tag{9}$$

where $\frac{D}{Dt} = \frac{\partial}{\partial t} + \mathbf{u}\cdot\nabla$ is the total derivative in time. First-order time derivatives can be computed directly by equations (3, 4) in their discrete form. The second-order derivatives are more complex expressions, which depend on partial tangential derivatives of Φ and $\partial\Phi / \partial n$ on Γ_{FS}. An improved method for the determination of these tangential derivatives is given in Fochesato et al. (2005c).

DIRECTIONAL WAVE FOCUSING

A flap snake wavemaker motion is specified at the inflow boundary Γ_{In} to focus different waves at a focal distance away from the wavemaker. The wavemaker motion is function of the transversal and vertical coordinates on the inflow boundary and describes the transient movement of the paddle in the normal direction.

In this paper, computations are carried out in a dimensionless coordinate system. The computational domain has a length of L_x=10.0, a width of L_y=20.0 and an initially undisturbed water surface with a constant water depth d=1.0. The discretization has been performed with 20 elements in x-direction, 40 elements in y-diretion and 4 elements in z-direction which results in approximately 2100 elements for the complete model.
At the inflow boundary Γ_{In} the snake wavemaker motion is defined by the superposition of 10 sinusoidal waves of frequency ω=1.2816. The direction of these waves varies within an angle of φ = -45° … +45° with respect to the x-axis. The different phase shifts for each particular wave are chosen to result in directional focusing of the energy at x=7.5 from the inflow boundary (assuming they propagate at the linear wave velocity). Figure 2 shows the free surface computed in the wave tank at time t=18.5. We see the appearance of a large wave the middle of the NWT. Downstream of this extreme wave, there is a so-called "hole in the sea", where the surface elevation drops below the still water level of z=0. In Figure 3 the x- and z-components of the velocity field within the wave are shown as vectors in the x-z plane at y=0 (center line). The transversal y-component of the velocity at y=0 is zero.

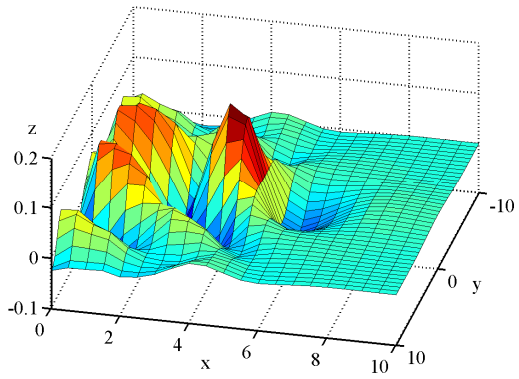

Fig. 2: Directional focusing at x~7.5 from inflow boundary at t=18.5

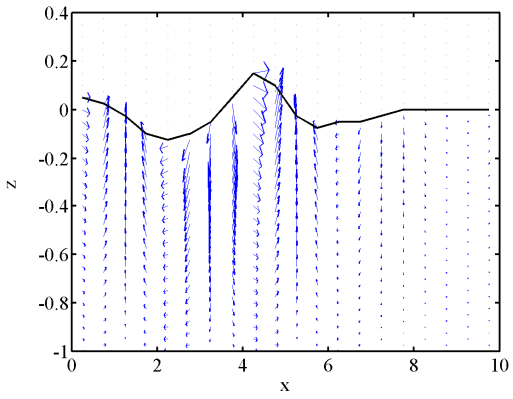

Fig. 3: Velocity field at center line (y=0) for t=18.5

WAVE SLAMMING AND PRESSURE IMPACT

When a steep extreme wave reaches a structure the structure is subjected to a short-duration high impact pressure depending on the shape of the structure and the shape of the wave. To determine the transient pressure distribution on the surface of a support structure, the fluid flow is modeled as a two-phase flow (water-air). The kinematics of the flow is described by the Navier-Stokes equations (viscous flow, equations (10, 11) below). The free surface is represented by the scalar volume fraction, which is transported through the domain by the wave flow field. The change of the spatial distribution of this scalar quantity is modeled by an advection equation (equation (14) below).

The discretization of the Navier-Stokes equations is performed by a finite volume method (FV). The advection equation for the volume fraction quantity to describe the interface (free surface) between the two fluids (air, water) is discretized by the volume of fluid method (VOF). The joint approach of finite volume method (FV) and the volume of fluid method (VOF) is labeled as finite volume – volume of fluid approach (FV-VOF).

$$\frac{\partial \rho}{\partial t} + \nabla \cdot (\rho \mathbf{U}) = S_{Mass} \tag{10}$$

$$\frac{\partial (\rho \mathbf{U})}{\partial t} + \nabla \cdot (\rho \mathbf{U} \circ \mathbf{U}) - \nabla \cdot (\mu (\nabla \mathbf{U} + [\nabla \mathbf{U}]^T)) = S - \nabla p \tag{11}$$

where

$$\rho = c_1 \rho_1 + c_2 \rho_2 \tag{12}$$

$$\mu = c_1 \mu_1 + c_2 \mu_2 \tag{13}$$

ρ_1 and ρ_2 are the constant densities of water and air, and μ_1 and μ_2 are the constant kinematic viscosities of water and air, respectively. c_1 and c_2=1.0-c_1 represent the volume fraction values of water and air (c_1 , c_2 ∈ [0;1]). Therefore, ρ and μ denote averaged quantities depending on the percentage of water and air at the considered position in the domain. This leads to a steady spatial distribution of fluid density and the kinematic fluid viscosity.

The free surface position is implicitly described by c_1 and is located at $c_1 = c_2 = 0.5$. The movement of the free surface depends on the fluid flow field and the corresponding change of the scalar field variable $c = c_1$ is governed by an advection equation

$$\frac{\partial c}{\partial t} + \mathbf{U} \cdot \nabla c = 0 \tag{14}$$

The discretization of equations (10), (11) and (14) is performed by a finite volume – volume of fluid method (FV-VOF). The 3D domain is discretized into polyhedral control volumes. Within each control volume, tri-linear ansatz functions are used in the spatial interpolation of the velocity components, the pressure and the volume fraction values. Diffusion terms are evaluated using derivatives of the interpolation functions. For the advective terms, an upwind scheme based on that of Barth and Jesperson (1989) is used. Transient terms are discretized using second-order Euler backward differencing.

WAVE IMPACT ON CIRCULAR CROSS-SECTION

In a first step the FV-VOF method is applied to determine the pressure evolution on the circumference of a circular cross-section due to the impact of an even height water front. The computational domain is shown in figure 4. A constant velocity v_{in} is defined on the inflow boundary and a constant pressure p_{ref} is defined on the outflow boundary. Wall boundary conditions are defined on the other boundaries (lateral boundaries and cylinder boundary: no normal flux; free slip). The initial velocity field is defined as [$v_{longitudinal}$; $v_{lateral}$]=[v_{in}=const ; 0]. The initial volume fraction field is defined such that an even wave front is located slightly upstream of the circular cross-section (figure 5).

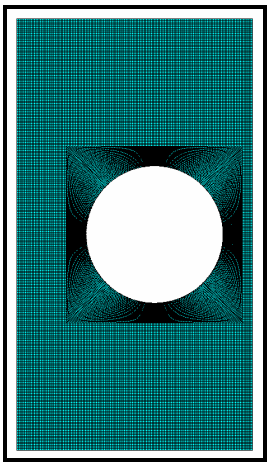

Fig. 4: Computational domain

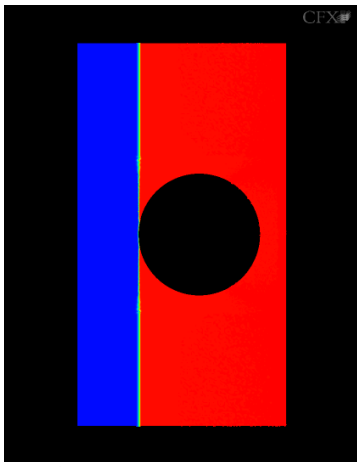

Fig. 5: Initial state (FVVOF)

The transient pressure evolution on the circumference is evaluated at positions A (φ = 0°), B (φ = 15°), C (φ = 30°) and D (φ = 60°), defined according to figure 6.

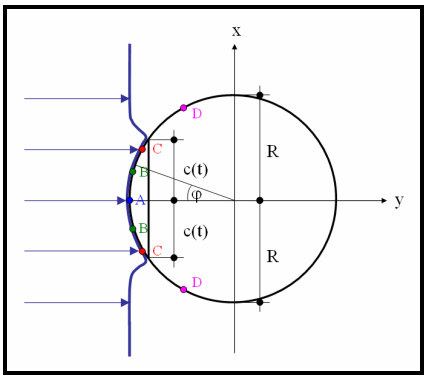

Fig. 6: Definition sketch for pressure evaluation

The computational results of the FV-VOF method are compared to the analytic method of Wienke (2001) (one-phase potential flow, constant fluid density ρ) and to experimental results by Wienke (2001) and Wienke and Oumeraci (2005). Figures 8-10 show the transient pressure evolution at positions A, B, and C, marked in figure 6. In all cases the maximum pressure computed with the FV-VOF method is smaller than that predicted by Wienke's method, which is due to the averaged density used in the FV-VOF model, by contrast with the potential flow approach of Wienke. Furthermore, unlike in the latter method, there is no pressure singularity for the FV-VOF model in figure 8 at t=0.
For later stages of the wave impact, both models (FV-VOF, Wienke) show good agreement with experimental results of Wienke (2001), Wienke and Oumeraci (2005). In all three diagrams (figures 8-10) the pressure maximum appears at nearly the same time for both models as in the experiments. Regarding the maximum pressure, there are slight differences between the two models on the one side, and between those and the experiments, on the other side. These differences are judged to be relatively small in comparison to the complexity of the measurements performed. For position D (φ = 60°; not shown) there is only qualitative agreement of the transient pressure distribution between the two models and the experimental results. But pressures at position D are one order of magnitude smaller than at position C (φ = 30°), and their contribution to the resulting force is thus negligeable.

Figures 11-13 show the radial distribution of the pressure (x: transversal coordinate; R: Radius; see figure 6) along the circumference of the cross-section, at times t_A=0.000R/V, when the wave front first touches the structure (V = v_{in} = const), t_B=0.011R/V and t_C=0.053R/V. Figure 11 clearly shows that there is no singularity in the pressure distribution at x=0 for the FV-VOF model. In Figures 12 and 13, for both models, the pressure maximum occurs approximately at the same radial position in good agreement with experimental data. For all radial pressure distributions, the FV-VOF model gives smaller maximum values for the pressure than the model of Wienke, as was already observed for the temporal pressure evolution (figures 8-10).

By integration of the pressure p(φ , t) around the circumference, the resulting line force f(t) in the flow direction can be obtained as:

$$f(t) = \int_{\varphi=-90°}^{\varphi=+90°} p(\varphi,t)\cos(\varphi)\, R\, d\varphi \qquad (15)$$

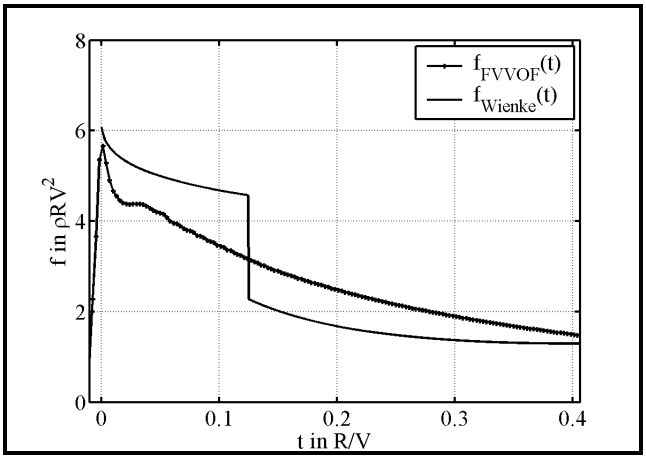

Fig. 7: Transient evolution of resulting line force

Figure 7 shows the resulting line force (integral of the pressure along the circumference of a circular cross-section) for the FV-VOF model and the analytic solution of Wienke (2001). The jump in the line force in the latter results from different approximation functions in the solution for the two different time regimes (t ≤ 0.125R/V ; t > 0.125R/V).

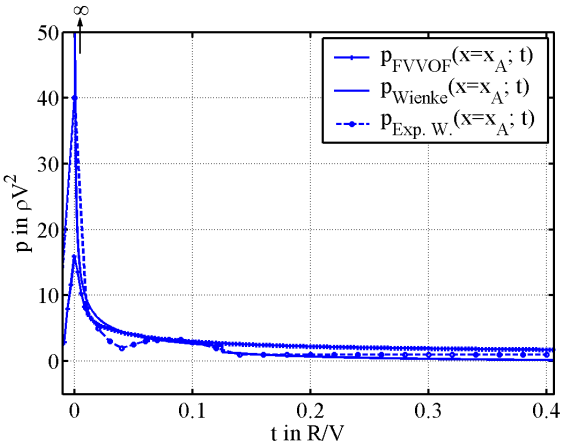

Fig. 8: Transient pressure evolution at position A

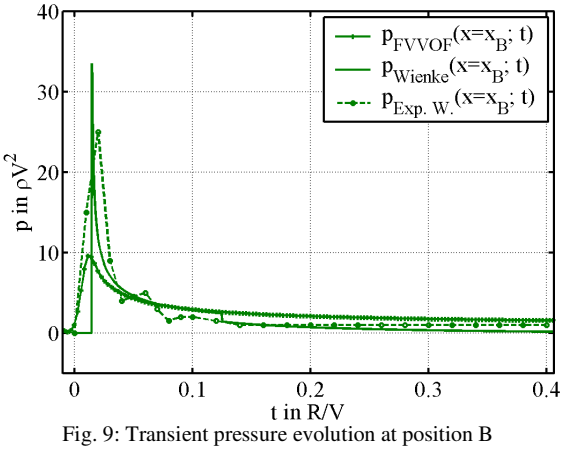

Fig. 9: Transient pressure evolution at position B

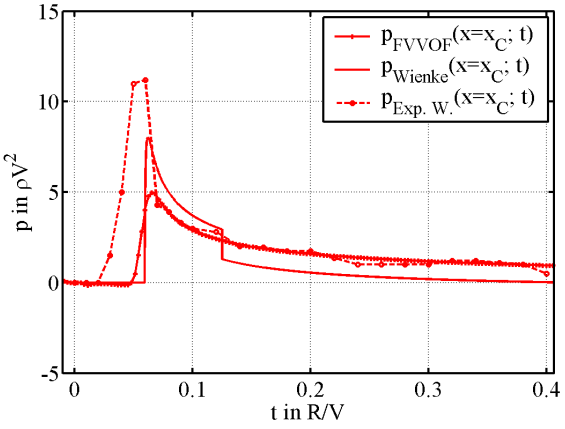

Fig. 10: Transient pressure evolution at position C

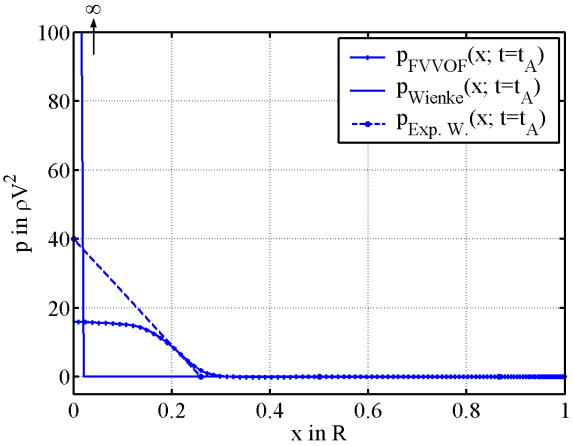

Fig. 11: Radial pressure distribution at $t = t_A$

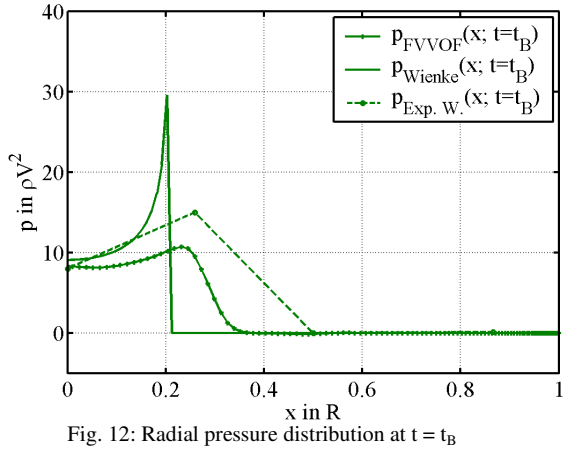

Fig. 12: Radial pressure distribution at $t = t_B$

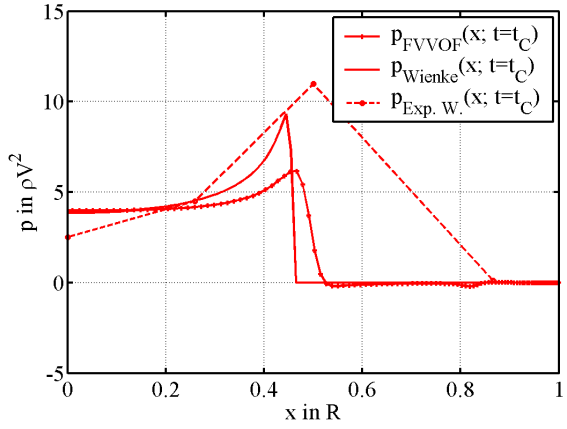

Fig. 13: Radial pressure distribution at $t = t_C$

In the FV-VOF computations the temporal evolution of the initially even water front is obtained along the circumference of the circular cross-section (see figure 6) from the variation of the volume fraction quantity. This evolution is compared in figure 14 to that from the model of Wienke and to experimental results. In the figure, the moistened width c(t) is plotted as a function of time and we see a good agreement of both models with the experimental results.

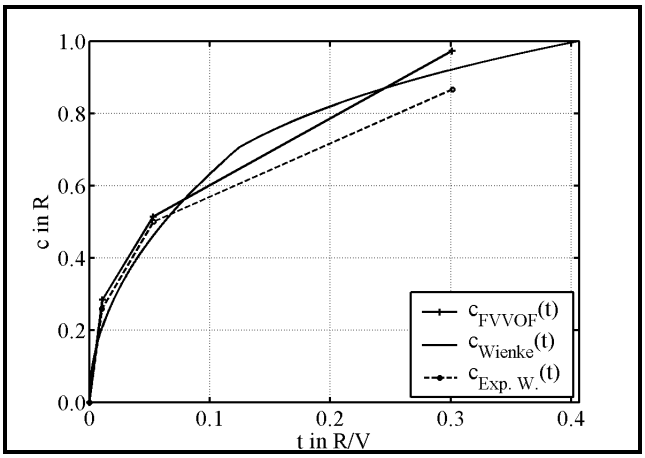

Fig. 14: Transient evolution of moistened width

3D FREAK WAVE IMPACT ON CYLINDRICAL SUPPORT STRUCTURE

In the extreme case of a 3D freak wave due, e. g., to directional energy focusing as in figure 2, impacting an offshore support structure, very high loads can result from the very high local hydrodynamic pressure. To determine such loads on a cylindrical support structure, the FNPF representation of a freak wave (figures 2-3) simulated in the BEM model is used as initial condition for the finite volume – volume of fluid model domain (FV-VOF). The FV-VOF discretization is performed as described above. At the initial state of the FV-VOF computation, downstream of the freak wave (figure 2, x~6.0), there is a marked decrease in surface elevation and, further downstream, the velocity field reaches nearly zero (see figure 3, $x \geq 6.0$). Accordingly, in the FV-VOF domain we position a cylinder of diameter D=0.5 at x~6.0, downstream of the freak wave, in the region not yet affected by the wave flow. Thus, upon restarting computations the slamming process of the wave onto the cylinder is simulated within the FV-VOF domain. To reduce computational cost, the FV-VOF domain is chosen smaller than the BEM domain in which the freak wave generation was simulated. The transient flow of the wave around the cylindrical structure is shown in figures 15-22 at different times t=19.5, …, t=23.0, where t=18.5 is the initial time for the FV-VOF computation.

While the wave flow overtakes the structure, the wave is obviously divided by the cylindrical obstacle. After the wave crest has passed the structure, remarkably the water fronts left and right of the cylinder change direction and diffract behind the cylinder to form an enhanced, refocused surface elevation directly behind the cylinder (figures 19-21). This peak in surface elevation directly downstream of the cylinder also causes an increased hydrostatic pressure on the downstream parts of the cylinder surface. Based on the pressure distribution computed on the cylinder surface, the resulting horizontal force and bending moment in the cylindrical support structure (e. g. with respect to the sea bottom) can be determined according to equation (15), with an extension to surface integration (also integration in vertical direction).

Figure 23 shows the transient horizontal force Q(t) and the transient bending moment M(t) thus obtained in the cylinder at the sea bottom level. According to figure 20, where we see a high surface elevation on the downstream half of the cylinder at approximate time t=22.0, the horizontal force and bending moment should reach maximum absolute value and be oriented in the upstream direction. As expected, we find $Q(t=22.0)<0$, and $M(t=22.0)<0$ in figure 23. Here, t is expressed in terms of $[d/g]^{1/2}$ (d: still water depth, g: gravitation), and Q(t) and M(t) in terms of $\rho V^2 R d$ and $\rho V^2 R d^2$, respectively (ρ: constant water density, R=D/2: radius of cylinder, $V=[gd]^{1/2}$: reference velocity).

CONCLUSIONS

In this paper we model the kinematics of extreme three-dimensional gravity waves in an NWT based on the free surface potential flow equations (fully nonlinear potential flow, FNPF). The 3D-NWT model is based on a higher-order boundary element method (BEM) for the spatial discretization and on a higher-order Eulerian-Langrangeian time integration scheme (Grilli et al. 2001). Improvements of the representation of higher-order time derivatives have been used here, following Fochesato et al (2005c). Freak wave generation has been performed as in Brandini and Grilli (2001), using a transient snake wavemaker motion at the inflow boundary, to superpose incoming sinusoidal waves of different angles, which results in wave energy focusing at a specified position downstream in the tank (directional focusing).

To model the pressure impact of extreme waves on offshore structures, such as cylindrical support structures, we used a finite volume – volume of fluid approach (FV-VOF) based on the Navier-Stokes equations for two-phase flow (water-air). The FV-VOF model was validated on a two-dimensional case, where an initially even water front hits a circular cross-section. Computational results were compared to an analytic model for one-phase potential flow and to experimental results. By contrast to the analytic model, however, the FV-VOF model is applicable to non-even incident waves of arbitrary surface shape and to arbitrary structures.

The transient load on a cylindrical tower/support structure is modeled by a combined approach using the 3D-BEM-NWT for the freak wave generation and the FV-VOF model for the wave slamming process, the latter model being initialized using results of the former model. Thus, the final state of the freak wave, close to breaking, generated in the BEM model is transferred to the 3D-FV-VOF domain, in which a cylinder has been positioned slightly downstream of the freak wave. The free surface flow of the freak wave around the cylinder is simulated in the FV-VOF model. Results show that, immediately after the wave crest has passed the structure, there is a high surface elevation on the downstream side of the cylinder and thus a high amount of (hydrostatic) pressure acting on the cylinder surface in the upstream direction. Accordingly, the resulting horizontal force and bending moment for the tower at sea bed level calculated for this time range are directed in the upstream direction as well.
The FV-VOF model can also be used for the case of a freak wave hitting an offshore support structure sideway, and can further be applied to multi-pile configurations of offshore support structures, where shadowing effects might lead to modified load combinations.

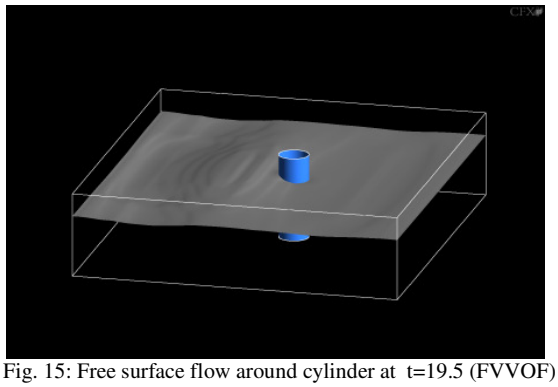

Fig. 15: Free surface flow around cylinder at t=19.5 (FVVOF)

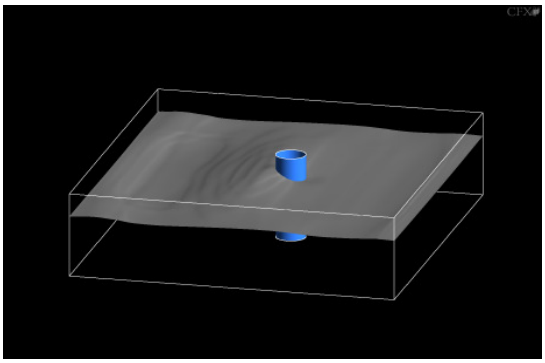

Fig. 16: Free surface flow around cylinder at t=20.0 (FVVOF)

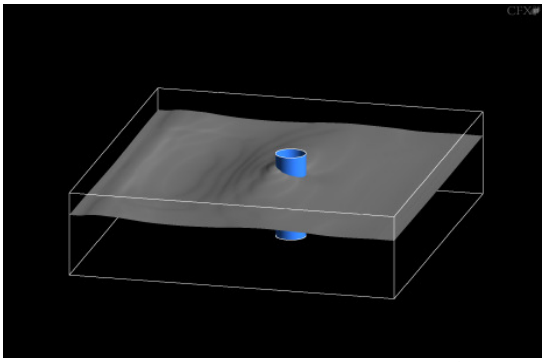

Fig. 17: Free surface flow around cylinder at t=20.5 (FVVOF)

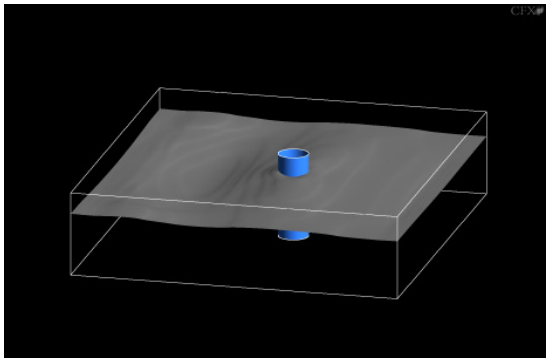

Fig. 18: Free surface flow around cylinder at t=21.0 (FVVOF)

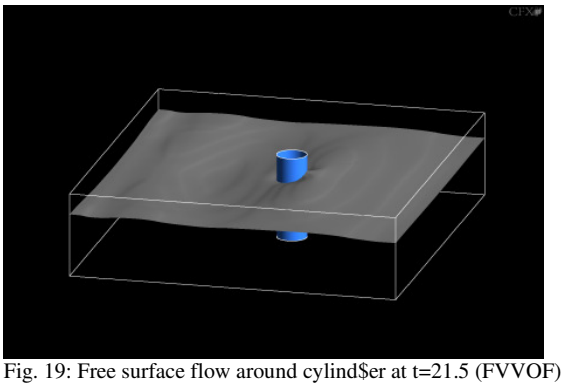

Fig. 19: Free surface flow around cylind$er at t=21.5 (FVVOF)

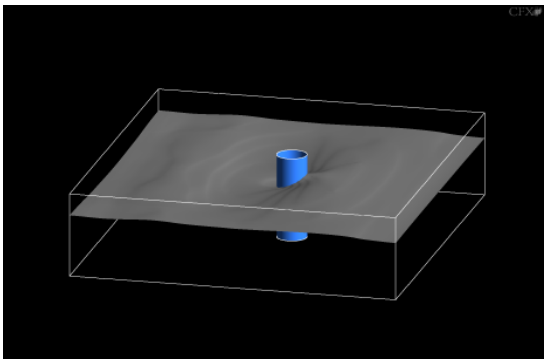

Fig. 20: Free surface flow around cylinder at t=22.0 (FVVOF)

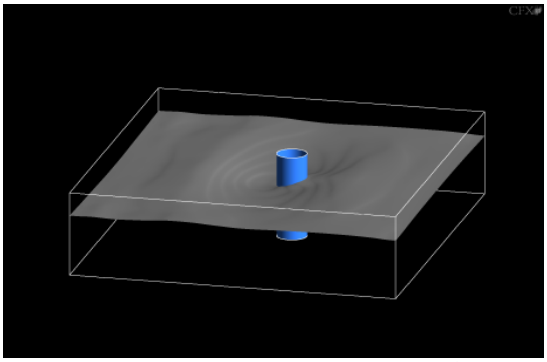

Fig. 21: Free surface flow around cylinder at t=22.5 (FVVOF)

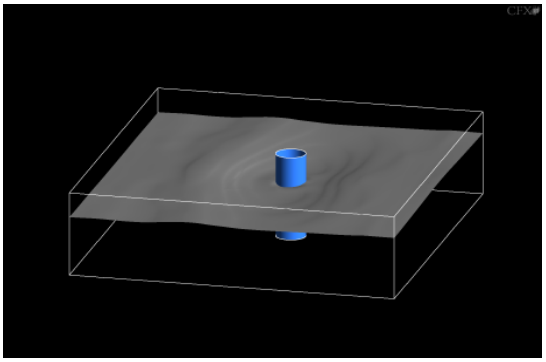

Fig. 22: Free surface flow around cylinder at t=23.0 (FVVOF)

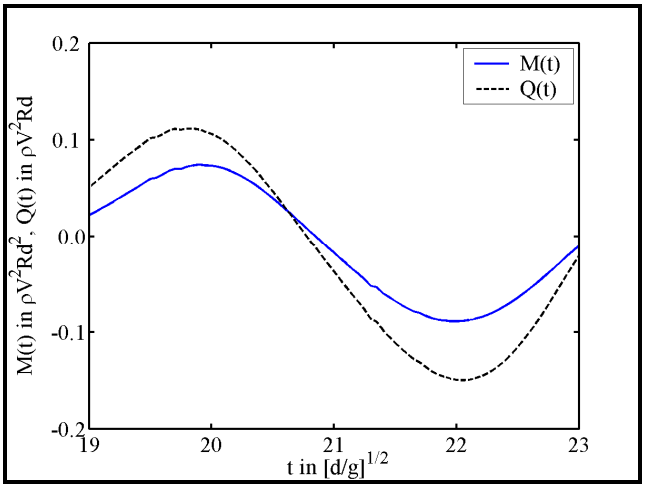

Fig. 23: Cylindrical support: freak wave-induced bending moment and horizontal force at the sea bottom

ACKNOWLEDGEMENTS

This work was carried out within the Graduate College "Fluid-Structure Interaction" (GRK 432) of the Deutsche Forschungsgemeinschaft (DFG) at Technische Universität Braunschweig, Germany. Financial support by Deutscher Akademischer Austauschdienst (DAAD) is gratefully acknowledged.

REFERENCES

Barth, T. J. and Jesperson, D. C. (1989). "The Design and Application of Upwind Schemes on Unstructured Meshes", *Report AIAA-89-0366, American Institute for Aeronautics and Austronautics.*

Fabula, A. G. (1957). "Ellipse-fitting approximation of two-dimensional, normal symmetric impact of rigid bodies on water", *Proc. 5th Midwestern Conference on Fluid Mechanics*, 299-315.

Fochesato, C., Dias, F. and Grilli, S. T. (2005a). "Wave Energy Focusing in a Three-dimensional Numerical Wave Tank", *Proc. 15th ISOPE Conf.*, 24-31.

Fochesato C., Dias F. and Grilli S.T. (2005b). "Wave Energy Focusing in a Three-dimensional Numerical Wavetank", *Proc. Rogue Waves 2004 Conf.* (Brest, France, June 2004).

Fochesato, C., Grilli, S. T. and Guyenne, P. (2005c). "Note on Non-Orthogonality of Local Curvilinear Co-ordinates in a Three-dimensional Boundary Element Method", *Intl. J. Num. Meth. In Fluids*, Vol. 48, 305-324.

Goda, Y. (1964). "Wave forces on a vertical circular cylinder: Experiments and a proposed method of wave force computation", Report No. 8, Port and Harbour Technical Research Institute.

Grilli, S. T. and Subramanya, R. (1994). "Quasi-singular Integrals in the Modeling of Nonlinear Water Waves in Shallow Water", *Engineering Analysis with Boundary Elements*, Vol. 13, 181-191.

Grilli, S. T. and Subramanya, R. (1996). "Numerical Modeling of Wave Breaking Induced by Fixed or Moving Boundaries", *Computational Mechanics*, Vol. 17, 374-391.

Grilli, S. T., Guyenne, P. and Dias, F. (2001). "A Fully Nonlinear Model for Three-Dimensional Overturning Waves over Arbitrary Bottom", *Int. Journ. Num. Meth. Fluids*, Vol. 35, 829-867.

Grilli, S. T., Fochesato, C. and Dias, F. (2005). "Wave Energy Focusing in a Three-dimensional Numerical Wavetank", *Proc. 5th Int. Symp. Ocean Wave Measurement and Analysis*, ASCE publications, paper 197.

Kharif, C. and Pelinovsky, E. (2003). "Physical Mechanisms on the Rogue Wave Phenomenon", *Eur. Journ. Mech. B-Fluids*, Vol. 22 (6), 603-634.

Wagner, H. (1932). "Über Stoß- und Gleitvorgänge an der Oberfläche von Flüssigkeiten", *Zeitschrift für Angewandte Mathematik und Mechanik*, Vol. 12 (4), 193-215.

Wienke, J. (2001). "Druckschlagbelastung auf schlanke zylindrische Bauwerke durch brechende Wellen – theoretische und gromaßstäbliche Laboruntersuchungen – ", Dissertation thesis, Technische Universität Braunschweig.

Wienke, J. and Oumeraci, H. (2005). "Breaking Wave Impact Force on a Vertical and Inclined Slender Pile – Theoretical and Large-scale Model Investigations", *Journ. Coastal Engineering*, Vol. 52, 435-462.